Birefringence-Directed Raman Selection Rules in 2D Black Phosphorus Crystals

Nannan Mao, Juanxia Wu, Bowen Han, Jingjing Lin, Lianming Tong, and Jin Zhang**

The incident and scattered light engaged in the Raman scattering process of low symmetry crystals always suffer from the birefringence-induced depolarization. Therefore, for anisotropic crystals, the classical Raman selection rules should be corrected by taking the birefringence effect into consideration. The appearance of the 2D anisotropic materials provides an excellent platform to explore the birefringence-directed Raman selection rules, due to its controllable thickness at the nanoscale that greatly simplifies the situation comparing with bulk materials. Herein, a theoretical and experimental investigation on the birefringence-directed Raman selection rules in the anisotropic black phosphorus (BP) crystals is presented. The abnormal angle-dependent polarized Raman scattering of the A_g modes in thin BP crystal, which deviates from the normal Raman selection rules, is successfully interpreted by the theoretical model based on birefringence. It is further confirmed by the examination of different Raman modes using different laser lines and BP samples of different thicknesses.

1. Introduction

Raman spectroscopy is a powerful tool to characterize the structure information of crystals.[1] Practically, the polarized Raman spectroscopy has been widely used to determine the crystalline orientation and degree of disorder, and to differentiate single crystal from polycrystalline materials.[2] However, for crystals with low symmetry, the polarization of both the incident laser and Raman-scattered light can be exclusively altered due to the birefringence effect of the crystal itself, so that the polarized Raman scattering always deviates significantly from the normal Raman selection rule.[3] Even though this abnormal polarized Raman behavior of the anisotropic crystals has been observed for many years,[3a,b,4] the influence of optical birefringence on the Raman selection rules of the anisotropic crystal itself has been rarely investigated even up to now. The key limitations are attributed to its considerable complexity with multitudinous influence factors for bulk crystals, such as the uncontrollable thickness, the uncertainty of the laser penetration depth, as well as the anisotropic absorption and reflection of the incoming and scattered light.[3d]

Recently, a new class of 2D anisotropic layered materials, such as black phosphorus (BP),[5] rhenium disulphide (ReS_2),[6] have been rediscovered as promising materials for electronics and optoelectronics. Owing to the unique atomic structures, they exhibit robust in-plane optical anisotropy with huge birefringence effect.[5b] Their optical properties, including absorption, fluorescence, and Raman scattering, have shown significant polarization dependence.[7] For the 2D layered materials, on one hand, the unique layered structures connected through van der Waals forces ensure that the thickness can be precisely controlled; on the other hand, the nanoscale thickness of the 2D material guarantees the certainty of the laser penetration depth. Therefore, the emergence of the layered BP, as well as other 2D anisotropic

N. Mao, Dr. J. Wu, B. Han, Dr. J. Lin, Dr. L. Tong, Prof. J. Zhang
Center for Nanochemistry
Beijing National Laboratory for Molecular Sciences
Key Laboratory for the Physics and Chemistry of Nanodevices
State Key Laboratory for Structural Chemistry of Unstable and Stable Species
College of Chemistry and Molecular Engineering
Peking University
Beijing 100871, P. R. China
E-mail: tonglm@pku.edu.cn; jinzhang@pku.edu.cn

DOI: 10.1002/smll.201600295

© 2016 Wiley-VCH Verlag GmbH & Co. KGaA, Weinheim

www.MaterialsViews.com

layered materials has brought new opportunities to explicitly investigate the influence of birefringence phenomenon on the polarized Raman spectra of the anisotropic crystals.

In the present study, we investigated the birefringence-directed Raman selection rule in the thin BP crystals. The abnormal polarized Raman scattering of the A_g^1 and A_g^2 modes in the BP crystals, which does not obey the normal Raman selection rules, can be successfully explained by the semi-quantitative model based on the birefringence effect. Meanwhile, by examining the A_g^1 and A_g^2 modes of the BP samples with different thicknesses using three excitation laser lines (488.0, 514.5, and 632.8 nm), we demonstrated that birefringence-directed Raman selection rule in the anisotropic material is dependent on three key factors, that is, the wavelength of the incident and scattered light, the thickness of the BP crystal, as well as particular types of Raman mode. Our work not only successfully explains the abnormal polarized Raman scattering of the 2D BP crystals, but also reveals a universal but little-known effect of birefringence on the polarized Raman scattering of nonpolar modes in the anisotropic crystals, such as crystals with orthorhombic, monoclinic, and triclinic symmetries.

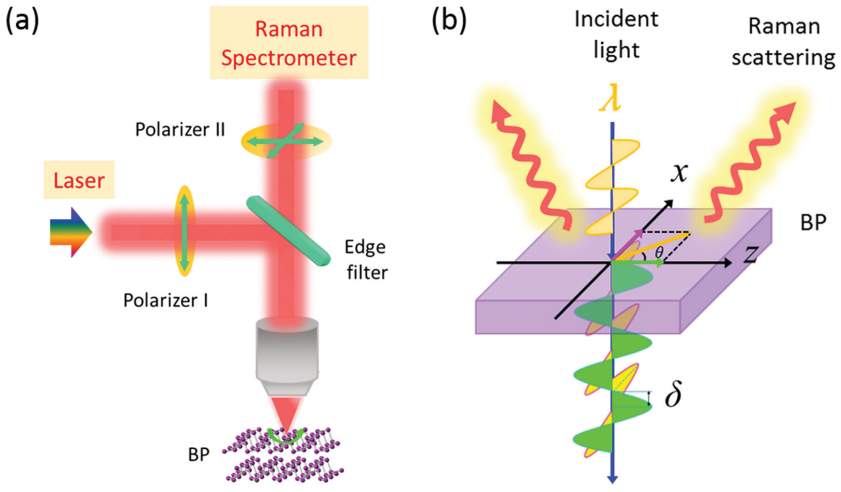

Figure 1. Experimental scheme and birefringence phenomenon in BP crystals. a) Schematic diagram of angle-resolved polarized Raman scattering of the BP sample. b) Schematic illustration of the birefringence effect in the BP crystal. The *x* and *z* axes are along the zigzag (ZZ) and armchair (AC) directions, respectively. θ is the angle between the AC direction and the polarization direction of the incident laser. The phase delay between the two components of the incident due to birefringence is represented by δ.

2. Results and Discussion

Figure 1a shows the experimental setup for the polarized Raman scattering of the BP samples. Raman spectra of BP were recorded in a backscattering geometry. Bulk BP belongs to the orthorhombic crystal system, and the complex refractive indices along the three orientation directions are totally different.[8] The birefringence in the BP crystal is illustrated in Figure 1b, when the linearly polarized laser vertically shines on the surface of the thin BP crystals, the polarization vector of the incident light can be decomposed into two components along the two crystalline orientation directions, that is, the zigzag (ZZ) (x) and armchair (AC) (z) directions, respectively. These two components propagate in the BP crystal with different phase velocities, and exit the sample with a phase difference δ. In Figure 1b, θ is the angle between the AC direction and the polarization direction of the incident laser.

Figure 2a shows top view of the atomic structure of the monolayer BP. According to the group theory, bulk BP crystal belongs to point group D_{2h}[18]. The primitive unit cell of bulk BP contains four atoms, represented by the dashed rectangle in Figure 2a. Hence, there are 12 phonon modes in the BP crystals: $\Gamma = 2A_g + B_{1g} + B_{2g} + 2B_{3g} + A_{1u} + 2B_{1u} + 2B_{2u} + B_{3u}$.[9] Six of them are Raman active and only the three modes A_g^1 (362 cm^{-1}), B_{2g} (439 cm^{-1}), and A_g^2 (468 cm^{-1}) are allowed in the backscattering geometry.[9a] The atomic displacements for these typical Raman modes are shown in Figure 2b. The Raman tensors of these modes are as follows[7a,d,9a]

$$\tilde{R}(A_g) = \begin{pmatrix} a & 0 & 0 \\ 0 & b & 0 \\ 0 & 0 & c \end{pmatrix} \qquad \tilde{R}(B_{2g}) = \begin{pmatrix} 0 & 0 & e \\ 0 & 0 & 0 \\ e & 0 & 0 \end{pmatrix} \tag{1}$$

Figure 2d shows the polarized Raman spectra of the sample shown in Figure 2c in the thick region (76 nm) when the sample is rotated under parallel polarization configuration. As reported previously, the Raman scattering of BP exhibits significant angle dependence.[5a,7] The A_g^2 mode shows the largest Raman intensity at 0° and 180°, and it decreases when the sample is rotated from 0° to 60°, then increases to a local maximum at 90°. The Raman intensity of A_g^1 mode does not show obvious variation during the rotation. For the B_{2g} mode, it disappears when the intensity of A_g^2 mode reaches a local maximum. According to the group theory, the Raman intensity for each mode can be calculated as

$$I \propto |e_i R e_s|^2 \tag{2}$$

where e_i and e_s are the polarization vectors of the incident and scattered light, respectively, and R stands for the Raman tensor for each Raman active mode.[1] For the isotropic layered materials such as graphene, h-BN, and MoS_2, e_i equals the polarization vectors of the electric fields for the incident light. However, for the anisotropic materials with high birefringence,[4] the actual e_i that interacts with the material is very different from

© 2016 Wiley-VCH Verlag GmbH & Co. KGaA, Weinheim

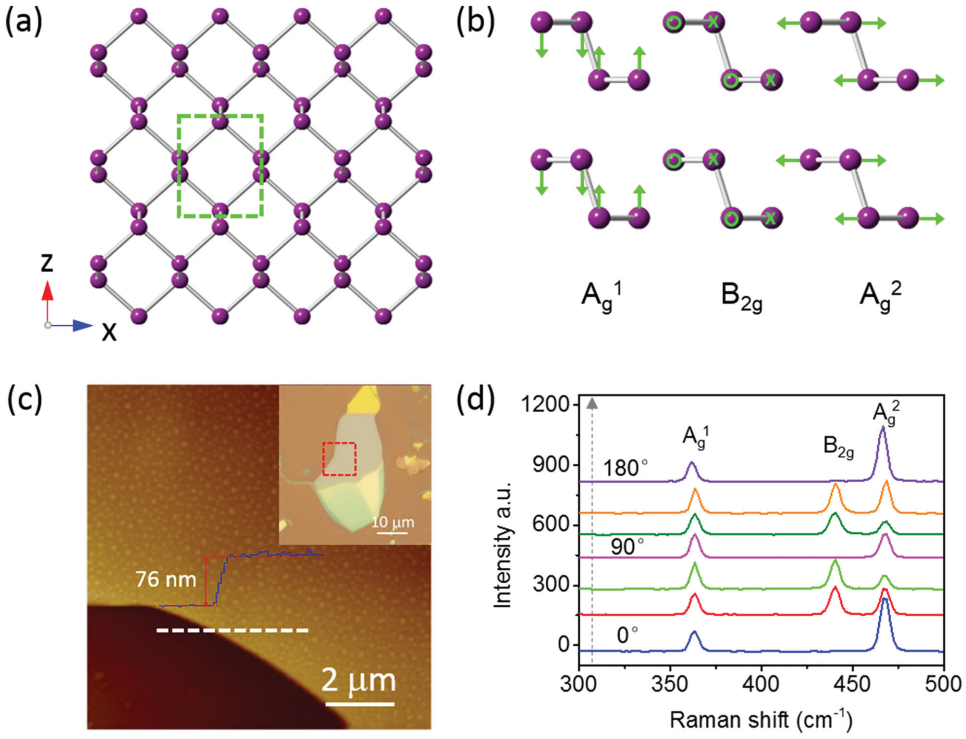

Figure 2. The atomic structure, typical Raman modes of BP, and AFM/OM/Raman characterization of a thin BP sample. a) Top view of monolayer BP with puckered layers. The *x* and *z* axes are the ZZ and AC directions, respectively. b) The atomic displacements for the three typical Raman modes A_g^1, B_{2g}, and A_g^2 in BP. c) Atomic force micrograph of the rectangular area in the inset, which is the optical micrograph of the BP sample on 300 nm SiO_2/Si substrate. d) Raman spectra of the BP crystal at different sample rotation angles. The wavelength of the excitation laser is 514.5 nm.

the original polarization vector of the incident light due to the birefringence phenomenon. Similarly, the scattered light also suffers from the birefringence effect when it exits from the crystal. Therefore, the polarized Raman scattering BP, as well as other anisotropic materials, should fully take into account the birefringence effect.[10] For simplicity, we assume normal incidence of the laser and neglect the anisotropic absorption in the BP crystal (see Supporting Information for more discussion).

The polarization vector of the incident light can be decomposed into two components, which are the electric fields along the AC (z) and ZZ (x) directions of the BP crystal, respectively, that is

$$e_{\mathbf{i}} = (\sin\theta\ 0\ \cos\theta) \tag{3}$$

or in the vector form

$$e_{\mathbf{i}} = \cos\theta \mathrm{r}_z + \sin\theta \mathrm{r}_x \tag{4}$$

where r_x and r_z are the unit vectors of electric fields along the ZZ and AC directions of the BP crystal. Owing to the birefringent property, they travel through the BP crystal at different velocities with a phase difference (δ). So the actual incident electric field that excites the Raman signals of BP is e_i' is

$$e_{\mathbf{i}}' = \cos\theta \cdot e^{-i\delta}\mathrm{r}_z + \sin\theta \mathrm{r}_x \tag{5}$$

The polarization of the scattered light (e_s'), just after the scattering event, is expressed as

$$e_{\mathbf{s}}' = Re_{\mathbf{i}}' \tag{6}$$

where R is the Raman tensor for the Raman mode.[1] For the A_g mode in the BP crystal

$$e_{\mathbf{s}}' = \begin{pmatrix} a & 0 & 0 \\ 0 & b & 0 \\ 0 & 0 & c \end{pmatrix}\begin{pmatrix} \sin\theta \\ 0 \\ \cos\theta e^{-i\delta} \end{pmatrix} = \begin{pmatrix} a\sin\theta \\ 0 \\ c\cos\theta e^{-i\delta} \end{pmatrix} \tag{7}$$

or in the vector form

$$e_{\mathbf{s}}' = c\cos\theta e^{-i\delta}\mathrm{r}_z + a\sin\theta \mathrm{r}_x \tag{8}$$

The scattered Raman signals undergo the same amount of phase difference δ since the wavelength of the Raman scattered light is very close to that of the excitation laser

$$e_{\mathbf{s}} = c\cos\theta e^{-2i\delta}\mathrm{r}_z + a\sin\theta \mathrm{r}_x \tag{9}$$

The polarized Raman intensity under parallel and cross polarization configurations can be calculated by decomposing e_s into directions parallel and perpendicular to e_i ($e_{i\parallel}$ and $e_{i\perp}$), respectively

© 2016 Wiley-VCH Verlag GmbH & Co. KGaA, Weinheim

www.MaterialsViews.com

Table 1. Raman scattering efficiency of A_g and B_{2g} modes.

Raman mode	Parallel polarization		Cross polarization	
	Case 1[a)]	Case 2[b)]	Case 1[a)]	Case 2[b)]
A_g mode	$(a\cos^2\theta + c\sin^2\theta)^2$	$a^2\sin^4\theta + c^2\cos^4\theta + 2ac\sin^2\theta\cos^2\theta\cos2\delta$	$(a-c)^2\sin^2\theta\cos^2\theta$	$\sin^2\theta\cos^2\theta(a^2 - 2ac\cos2\delta + c^2)$
B_{2g} mode	$e^2\sin^2 2\theta$	$e^2\sin^2 2\theta$	$e^2\cos^2 2\theta$	$e^2\cos^2 2\theta$

[a)]Without and; [b)]with considering birefringence in BP crystal, respectively.

$$e_{i\parallel} = (\sin\theta\ 0\ \cos\theta) \quad (10)$$

$$e_{i\perp} = (\cos\theta\ 0\ -\sin\theta) \quad (11)$$

Therefore, $I_{\parallel}$ and $I_{\perp}$ for A_g Raman mode in BP crystal (also see **Table 1**) can be given by

$$I_{\parallel} = a^2\sin^4\theta + c^2\cos^4\theta + 2ac\cos^2\theta\sin^2\theta\cos2\delta \quad (12)$$

$$I_{\perp} = \sin^2\theta\cos^2\theta(a^2 - 2ac\cos2\delta + c^2) \quad (13)$$

For the nonpolar mode (A_g mode) in BP crystals, the Raman efficiency is apparently different when the birefringence is taken into consideration. The Raman efficiency for B_{2g} is the same for both situations (Table 1).

Figure 3a,b shows the Raman scattering intensities of the B_{2g} and A_g^2 modes as a function of the sample rotation angle θ under parallel polarization configuration, respectively. It is seen that the B_{2g} mode shows a periodic pattern with 90° period. The intensity is minimum at 0°, 90° and 180°, that is, with laser polarization parallel to the crystalline orientations of BP, and maximum at 45°. This is in good agreement with the theoretical prediction (the solid curve in Figure 3a) in Table 1, which shows that the birefringence does not affect the B_{2g} mode. The A_g^2 mode in Figure 3b exhibits maxima at 0° and 180° when the laser polarization is parallel to the AC direction of BP. However, it also exhibits second maxima at 90° and 270° with the laser polarization parallel to the ZZ direction, which is consistent with the previous experimental observations.[7a,10] This cannot be explained by the normal Raman tensor analysis (case 1, parallel configuration in Table 1) which predicts maxima at 0°/180° and minima at 90°/270° (see Figure S2, Supporting Information). However, by incorporating the phase delay due to birefringence, the experimental data in Figure 3b can now be nicely fitted by Equation (12), as shown by the solid curve. Furthermore, by fitting these experimental results under parallel polarization (Figure 3a,b), we can get the apparent absolute values of the Raman tensor elements a, c, e, and the phase difference δ in Equation (12). Substituting these values into Equation (13), we now obtain the Raman intensity as a function of rotation angle under cross polarization. The results were plotted in Figure 3c,d (green curves) along with our experimental data

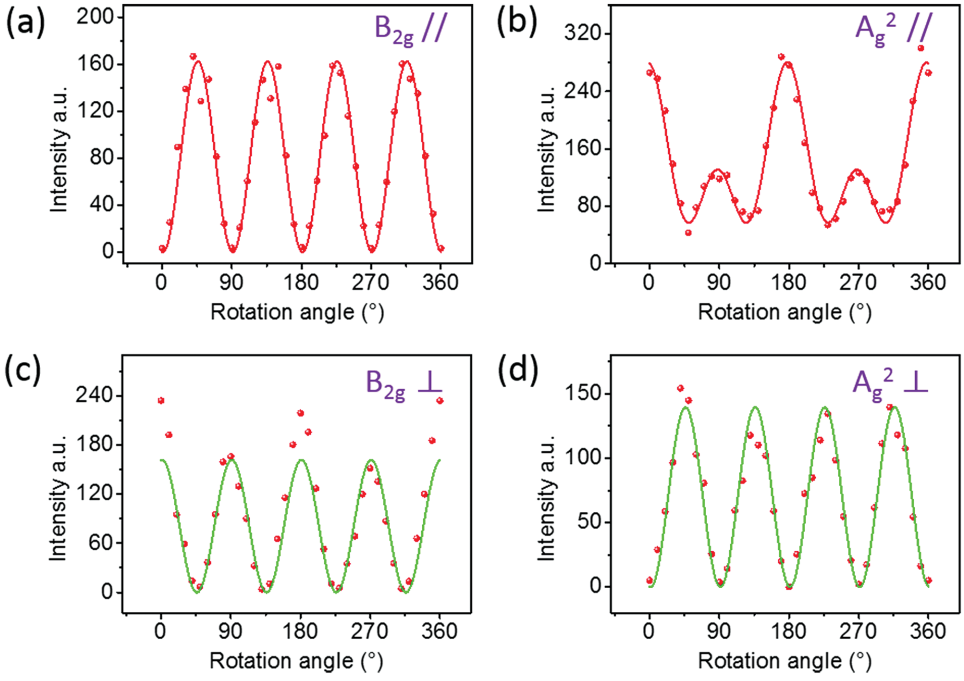

Figure 3. The Raman intensities of the A_g^2 and B_{2g} modes as a function of the sample rotation angle. a,b) Angle-dependent intensities of the (a) B_{2g} and (b) A_g^2 modes under parallel polarization. Solid lines are the fitting results using the model considering birefringence in Table 1. c,d) Angle-dependent Raman intensities of the (c) B_{2g} and (d) A_g^2 modes under cross polarization. Red dots and green lines represent the experimental and calculated results. The wavelength of the excitation laser was 514.5 nm.

© 2016 Wiley-VCH Verlag GmbH & Co. KGaA, Weinheim

(red dots). It is clear that the calculated intensities of A_g^2 are in excellent agreement with experimental data, represented by the red dots, not only in the periodic trend but also in the absolute intensities at different rotation angles. For the B_{2g} mode in Figure 3c, we see that the experimental data showed local maxima at 90° and 270° that are lower than the maxima at 0° and 180°. This is attributed to the anisotropic absorption of BP, and can be well-fitted by introducing the different anisotropic absorption efficiencies of the incident and scattered light along the AC and ZZ crystalline directions, respectively. Since the variation trend of the calculated Raman efficiency for the A_g^2 mode under parallel polarization is the same in the two situations whether we consider the anisotropic absorption in BP crystals or not (Figures S3 and S4, Supporting Information), we concluded that it is birefringence not anisotropic absorption that mainly causes the abnormal polarized Raman scattering of A_g^2 mode. Meanwhile, the anisotropic absorption affects only the amplitudes, not the trend of the Raman intensity curves of A_g^2 mode (see details in Supporting Information).

The phase difference between the two components along the AC and ZZ directions due to birefringence can be estimated as

$$\delta = \frac{2\pi}{\lambda}(n_z - n_x)\Delta d \tag{14}$$

where λ is the wavelength, and n_x, n_z are the complex refractive indices of BP along the ZZ and AC directions, respectively. The thickness of the BP sample is represented by Δd. In fact, the phase difference in practice is far more complicated than Equation (14) due to the oblique incidence of light focused by the objective lens,[11] the anisotropic absorption and reflection processes,[3d] and the multilayer interference.[12] Although it is hard to quantitatively calculate the actual δ, Equation (14) supplies a semi-quantitative description and reveals the three determinant factors, λ, n, and Δd.

To further investigate the birefringence-directed Raman selection rule in BP crystals, we studied the effect of incident wavelength, sample thickness, and different Raman modes, as illustrated in **Figure 4**a,c,e. In Figure 4b, we show the angular

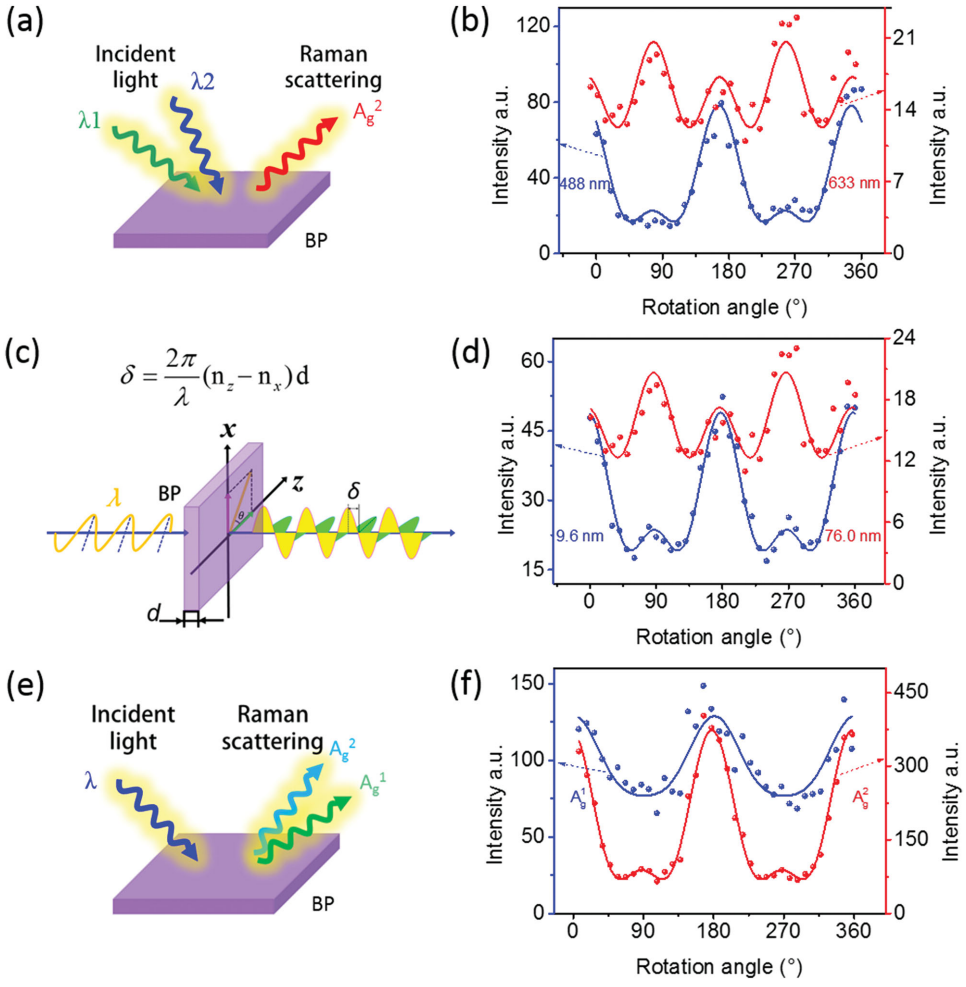

Figure 4. Birefringence-directed Raman selection rules of the BP crystal. a,c,e) Schematic illustration for the three key factors determining the birefringence effect in polarized Raman scattering of BP: a) the incident wavelength (λ, n), c) BP thickness (d), and e) the Raman modes (λ, n). The phase difference in BP is determined by the refractive index (n), wavelength (λ), and thickness (d). b,d,f) The angle-dependent Raman intensity of A_g modes under parallel polarization: b) A_g^2 mode for thick BP (76 nm) with excitation of 488.0 nm (blue line) and 632.8 nm (red line) laser; d) A_g^2 mode for the thin (9.6 nm, blue line) and thick (76 nm, red line) BP regions with excitation of 632.8 nm laser; f) Both of A_g^1 (blue line) and A_g^2 (red line) Raman modes for thin BP region with excitation of 514.5 nm laser. The solid lines are the fitting results using Equation (12).

© 2016 Wiley-VCH Verlag GmbH & Co. KGaA, Weinheim

Table 2. The dependence of the fitted anisotropic factor (a/c) on the laser wavelength, the thickness of the BP sample, and the Raman modes, using Equation (12).

a/c	Thin region (9.6 nm)		Thick region (70 nm)	
	A_g^1	A_g^2	A_g^1	A_g^2
488.0 nm		2.33		1.86
514.5 nm	1.29	2.05		1.47
632.8 nm		1.44	0.70	0.91

dependence of A_g^2 Raman modes for the same BP sample (thick region, 76 nm) with excitation wavelengths 488.0 nm (blue dots) and 632.8 nm (red dots), and the corresponding fitting results (solid curves) using the above model, respectively. Excited by 632.8 nm laser, the Raman intensity of A_g^2 mode shows the maxima at 90° and 270°, and the second maxima at 0° and 180°, respectively, significantly different from that excited by 488.0 nm (and 514.5 nm, see Figure 2b). This gives the anisotropic factor, defined as a/c, smaller than one under 632.8 nm excitation. By contrast, the anisotropic factors of 488.0 and 514.5 nm for the same sample are larger than one, as listed in **Table 2**. This is attributed to the different dependence of the Raman tensor element on the excitation energy. Besides, the fitted phase delay can also be obtained and shown in **Table 3**. As the anisotropic refractive indices are wavelength-dependent, the phase delay differs for different excitation wavelengths, following the trend $\delta_{514.5\ nm} > \delta_{488.0\ nm} > \delta_{632.8\ nm}$. This matches well with the calculated phase difference using transfer matrix method (Figure S8, Supporting Information). Figure 4c illustrates the thickness-dependent phase difference for the polarized Raman scattering excited by 632.8 line. Here in Figure 4d, we compared the angle-dependent Raman scattering of A_g^2 mode for the thin and thick region (Figure 2c and Figure S1, Supporting Information) with the same crystalline orientation. The phase difference for 76 nm-thick BP sample is slightly larger than that for the thin sample (9.6 nm). Meanwhile, the anisotropic factor a/c is also thickness-dependent, as shown in Table 2.

As the wavelength of the Stokes–Raman scattered light is different from that of the laser, the phase delay is also different, although it is ignored in the previous model for the purpose of simplicity. Figure 4f shows the angle-dependent polarized Raman intensity of the A_g^1 and A_g^2 modes in thin BP region under the excitation of 514.5 nm laser. The fitted δ value for A_g^2 mode is larger than that for A_g^1 mode (Table 3). Even though the polarizations of the incident and scattered light for the two A_g modes are the same, the wavelength of the scattered light differs a little from each other. For example, the A_g^1 and A_g^2 modes at 467cm^{-1} correspond to 524.1 nm and 526.8 nm for 514.5 nm excitation. Meanwhile, the complex dielectric constants at different wavelength are also diverse. Hence, A_g^1 and A_g^2 modes for the same sample exhibit obviously different δ values under the equal experimental condition. In addition, we measured another BP sample which is much thicker, the theory still holds (see the experimental details in Figures S5 and S6 and Table S1, Supporting Information).

Table 3. The dependence of the fitted phase differences (δ) on the laser wavelength, the thickness of the BP sample, and the Raman modes, using Equation (12).

δo	Thin region (9.6 nm)		Thick region (70 nm)	
	A_g^1	A_g^2	A_g^1	A_g^2
488.0 nm		42 ± 4		46 ± 3
514.5 nm	16 ± 6	45 ± 2		56 ± 2
632.8 nm		38 ± 1		36 ± 2

For the 2D materials on SiO_2/Si substrate, the interference effect in the 300 nm thick-silicon dioxide layer enhances the Raman signals.[13] To confirm that the interference enhancement is not a decisive factor for birefringence-directed Raman selection rule, we measured the polarized Raman scattering of the BP layer on fused silica. The abnormal polarized Raman scattering also appeared for BP on the fused silica substrate, and can also be well explained by the above model (see the experimental details in Figure S7, Supporting Information). Similarly, the fitted phase difference and anisotropic factor (a/c) are also dependent on the excitation energy as well as the particular Raman mode (Table S2, Supporting Information). Comparing the cases of the SiO_2/Si and fused silica, we conclude that the interference effect in the SiO_2 film on Si is not the determinant factor in the abnormal behavior of polarized Raman scattering.

3. Conclusion

In conclusion, by taking into account the birefringence effect, we have successfully interpreted the abnormal polarized Raman scattering of A_g mode in the BP crystal. Meanwhile, a semi-quantitative model based on the birefringence effect was put up with, which illustrated the influence of the optical birefringence on the Raman selection rule in 2D anisotropic BP crystals. Furthermore, we demonstrated that the birefringence-directed Raman selection rules in BP crystals are dependent on three key parameters, that is, the excitation wavelength, the thickness of the BP crystal, and the types of Raman modes. Our work reveals a universal but little-known effect of birefringence phenomenon on the polarized Raman scattering in few-layered anisotropic BP crystals, we believe the same treatment should be considered when dealing with the polarized Raman scattering of the nonpolar modes in crystals with orthorhombic, monoclinic, or triclinic symmetries.

4. Experimental Section

BP samples used in this work were mechanically exfoliated from bulk BP crystals (Smart element) on 300 nm SiO_2/Si substrate. The optical microscope (BX51) and the atomic force microscope (Dimension 3100) were used to locate the BP layers and determine the thickness of the samples. The polarized Raman spectra were carried on HR 800 (Jobin Yvon Horiba), with the excitation of

© 2016 Wiley-VCH Verlag GmbH & Co. KGaA, Weinheim

three lasers 488.0, 514.5, and 632.8 nm focused by a 100× objective (0.9 NA). Raman signals were detected on a thermoelectrically cooled CCD (Synapse CCD) detector. The intensity of the laser was less than 100 μW to avoid damaging the BP samples. For parallel and cross polarization configurations of the Raman experiment, a polarizer (polarizer I) was placed in the incident path of the Raman instrument, and the analyzing polarizer (polarizer II) was situated before the spectrometer. Polarized I keeps vertical all the time to ensure that the incident polarized light is the same while polarization II can select the scattered light in the horizontal or vertical polarization direction.

Supporting Information

Supporting Information is available from the Wiley Online Library or from the author.

Acknowledgements

This work was supported by NSFC (Grants Nos. 21233001, 21129001, 51272006, 51432002, 51121091, 11374355, and 21573004) and MOST (2011YQ0301240201 and 2011CB932601) and China Postdoctoral Science Foundation (2015M580010).

[1] R. Loudon, *Adv. Phys.* **1964**, *13*, 423.
[2] a) J. C. Heckel, A. L. Weisman, S. T. Schneebeli, M. L. Hall, L. J. Sherry, S. M. Stranahan, K. H. DuBay, R. A. Friesner, K. A. Willets, *J. Chem. Phys. A* **2012**, *116*, 6804; b) M. Y. Huang, H. G. Yan, C. Y. Chen, D. H. Song, T. F. Heinz, J. Hone, *Proc. Natl. Acad. Sci. USA* **2009**, *106*, 7304; c) M. N. Iliev, D. Mazumdar, J. X. Ma, A. Gupta, F. Rigato, J. Fontcuberta, *Phys. Rev. B* **2011**, *83*, 014108.
[3] a) S. P. S. Porto, J. A. Giordmaine, T. C. Damen, *Phys. Rev.* **1966**, *147*, 608; b) C. K. Asawa, R. A. Satten, O. M. Stafsudd, *Phys. Rev.* **1968**, *168*, 957; c) A. Chaves, S. P. S. Porto, *Solid State Commun.* **1972**, *10*, 1075; d) A. Gozar, *Phys. Rev. B* **2002**, *65*, 176403.
[4] P. Alonso-Gutiérrez, M. L. Sanjuán, M. C. Morón, *Phys. Rev. B* **2005**, *71*, 085205.
[5] a) F. N. Xia, H. Wang, Y. C. Jia, *Nat. Commun.* **2014**, *5*, 4458; b) J. S. Qiao, X. H. Kong, Z. X. Hu, F. Yang, W. Ji, *Nat. Commun.* **2014**, *5*, 4475; c) H. Liu, Y. C. Du, Y. X. Deng, P. D. Ye, *Chem. Soc. Rev.* **2015**, *44*, 2732; d) Z. Luo, J. Maassen, Y. X. Deng, Y. C. Du, R. P. Garrelts, M. S. Lundstrom, P. D. Ye, X. F. Xu, *Nat. Commun.* **2015**, *6*, 8572.
[6] a) D. A. Chenet, O. B. Aslan, P. Y. Huang, C. Fan, A. M. van der Zande, T. F. Heinz, J. C. Hone, *Nano Lett.* **2015**, *15*, 5667; b) D. Wolverson, S. Crampin, A. S. Kazemi, A. Ilie, S. J. Bending, *ACS Nano* **2014**, *8*, 11154; c) S. Tongay, H. Sahin, C. Ko, A. Luce, W. Fan, K. Liu, J. Zhou, Y.-S. Huang, C.-H. Ho, J. Yan, D. F. Ogletree, S. Aloni, J. Ji, S. S. Li, J. B. Li, F. M. Peeters, J. Q. Wu, *Nat. Commun.* **2014**, *5*, 4252.
[7] a) J. X. Wu, N. N. Mao, L. M. Xie, H. Xu, J. Zhang, *Angew. Chem. Int. Ed.* **2015**, *54*, 2366; *Angew. Chem.* **2015**, *127*, 2396; b) H. B. Ribeiro, M. A. Pimenta, C. J. de Matos, R. L. Moreira, A. S. Rodin, J. D. Zapata, E. A. de Souza, A. H. Castro Neto, *ACS Nano* **2015**, *9*, 4270; c) W. L. Lu, X. M. Ma, Z. Fei, J. G. Zhou, Z. Y. Zhang, C. H. Jin, Z. Zhang, *Appl. Phys. Lett.* **2015**, *107*, 021906; d) X. Ling, L. B. Liang, S. X. Huang, A. A. Puretzky, D. B. Geohegan, B. G. Sumpter, J. Kong, V. Meunier, M. S. Dresselhaus, *Nano Lett.* **2015**, *15*, 4080; e) S. Zhang, J. Yang, R. J. Xu, F. Wang, W. F. Li, M. Ghufran, Y. W. Zhang, Z. F. Yu, G. Zhang, Q. H. Qin, Y. R. Lu, *ACS Nano* **2014**, *8*, 9590.
[8] a) H. Asahina, A. Morita, *J. Phys. C: Solid State Phys.* **1984**, *17*, 1839.
[9] a) S. Sugai, T. Ueda, K. Murase, *J. Phys. Soc. Jpn.* **1981**, *50*, 3356; b) S. Sugai, I. Shirotani, *Solid State Commun.* **1985**, *53*, 753.
[10] J. Kim, J. U. Lee, J. Lee, H. J. Park, Z. Lee, C. Lee, H. Cheong, *Nanoscale* **2015**, *7*, 18708.
[11] M. Schubert, *Phys. Rev. B* **1996**, *53*, 4265.
[12] Z. H. Ni, H. M. Wang, J. Kasim, H. M. Fan, T. Yu, Y. H. Wu, Y. P. Feng, Z. X. Shen, *Nano Lett.* **2007**, *7*, 2758.
[13] a) S. Roddaro, P. Pingue, V. Piazza, V. Pellegrini, F. Beltram, *Nano Lett.* **2007**, *7*, 2707; b) Y. Y. Wang, Z. H. Ni, Z. X. Shen, H. M. Wang, Y. H. Wu, *Appl. Phys. Lett.* **2008**, *92*, 043121; c) X. Ling, J. Zhang, *J. Phys. Chem. C* **2011**, *115*, 2835.

Received: January 28, 2016
Revised: March 1, 2016
Published online: March 31, 2016

© 2016 Wiley-VCH Verlag GmbH & Co. KGaA, Weinheim